Mn_3O_4@$CoMn_2O_4$-CoO nanoparticles as active, stable and low-cost bifunctional electrocatalysis for ORR and OER

Zhishan Luo[†,‡], Erdem Irtem[†,‡], Raquel Nafria[†], Maria Ibáñez[⊥,‖], Sara Marti[¶], Maria Mata[¶], Yu Liu[†], Doris Cadavid[†], Jordi Llorca[¤], Jordi Arbiol[¶,¥], Teresa Andreu[†], Joan Ramon Morante[†,§], Andreu Cabot[†,¥,*]

[†] Catalonia Energy Research Institute - IREC, Sant Adrià del Besòs, Barcelona, 08930, Spain.

[⊥]Institute of Inorganic Chemistry, Dep. of Chemistry and Applied Biosciences, ETH Zürich, CH-8093, Switzerland

[‖]Empa-Swiss Federal Laboratories for Materials Science and Technology, Dübendorf, CH-8600, Switzerland

[¤] Universitat Politecnica de Catalunya

[¶] Institut Català de Nanociència i Nanotecnologia, ICN2, Campus de la UAB, 08193 Bellaterra, Spain.

[§] Departament d'Electronica, Universitat de Barcelona, 08028 Barcelona, Spain.

[¥]Institució Catalana de Recerca i Estudis Avançats - ICREA, 08010 Barcelona, Spain.

Supporting Information Placeholder

ABSTRACT: Mn_3O_4@$CoMn_2O_4$ nanoparticles (NPs) with adjustable composition were produced at low temperature and ambient atmosphere using a one-pot two-step synthesis protocol involving the cation exchange of Mn by Co in preformed Mn_3O_4 NPs. Selecting the proper cobalt precursor, CoO crystallites could be simultaneously nucleated on the NP surface to form Mn_3O_4@$CoMn_2O_4$–CoO. Such heterostructured NPs exhibited improved performance and durability as bifunctional catalysts for the oxygen reduction and evolution reactions (ORR, OER) over commercial Pt and IrO_2-based catalysts and over previously reported spinel electrocatalysts in alkaline solution.

The development of highly active, low overpotential, stable and low-cost electrocatalysts based on abundant and conflict-free raw materials is a critical challenge in several energy conversion technologies.[1] In particular, high performance bifunctional electrocatalysts for ORR and OER are an essential component in rechargeable metal-air batteries and regenerative low temperature fuel cells. In these devices, the use of a catalyst based on scarce and high cost Pt and platinum group metals represents a severe resource and cost constraint that strongly limits deployment.[2] Alternative cost-effective and abundant transition metal oxides have been recently shown as outstanding candidates for ORR and/or OER in alkaline media, showing excellent stability, very high activity, low overpotential and large roundtrip efficiency associated with their multiple possible oxidation states, off-stoichiometric compositions, defects and vacancies.[3-5] However, the multiple valence s and related structural variability at the origin of this outstanding electrocatalytic performance is also behind the difficulty to produce these compounds in a reproducible and controlled manner. This is a particularly important limitation when taking into account that the physicochemical properties of transition metal oxides are highly sensitive to composition, structural parameters and distribution and oxidation state of cations. Thus, while numerous works have recently analyzed the ORR/OER performance of a variety of transition metal oxides, a wide range of results, associated to a diversity of compositions and phases not always unequivocally determined, have been reported.[6]

Among the large variety of transition metal oxides, Mn-based spinels have shown particularly outstanding performance for ORR. Besides, Co-based oxides are also excellent electrocatalysts for ORR, but especially for OER. We hence anticipate the combination of Mn and Co oxides could result in bifunctional catalysts with substantially improved activity for both ORR and OER. Besides performance, to ensure relevance, materials need to be produced with large surface areas to maximize activity, and at a low cost, what requires the synthesis of NPs using low synthesis temperatures and ambient pressures.

In this work, we detail a scalable, low temperature and ambient pressure protocol to produce monodisperse Mn_3O_4@$CoMn_2O_4$ and Mn_3O_4@$CoMn_2O_4$-CoO NPs with controlled composition and phase distribution, and measure their performance toward ORR and OER.

Mn-Co oxide (MC) NPs were prepared by a one pot, two-step process. First Mn_3O_4 NPs with octahedral geometries were produced by decomposing $Mn(OAc)_2$ at 90 °C in the presence of oleylamine, oleic acid and water.[7] In a second step, within the same flask and at the same temperature, an aqueous cobalt chloride ($CoCl_2{\cdot}6H_2O$) solution was added and allowed to react for 300 min (supporting information, SI). Figures 1a and 1b show representative transmission electron microscopy (TEM) micrographs of the initial Mn_3O_4 and the MC NPs produced after adding an equivalent molar amount

of Co chloride ([Co]/[Mn]=1; MC1-Cl). Upon Co addition, the initial octahedral-shape Mn_3O_4 NPs were slightly rounded (Figure 1a-b) without undergoing any evident growth even for [Co]/[Mn] ratios up to 5. High-angle annular dark field scanning TEM (HAADF-STEM) in combination with electron energy loss spectroscopy (EELS) showed a core-shell type Co and Mn distribution with core and shell compositions compatible with Mn_3O_4 and $CoMn_2O_4$ stoichiometries, respectively (Figure 1c). All Co concentrations with [Co]/[Mn] above one resulted in similar core-shell type structures, with similar shell thickness. High resolution TEM (HRTEM) analysis showed the MC1-Cl NPs to have a body centered tetragonal Mn_3O_4 phase (space group = $I4_1/amd$) with lattice parameters a = b = 0.5718 nm and c = 0.9208 nm (SI). Satellite spots could be clearly identified, which upon filtering evidenced the presence of an epitaxial shell with a slight difference in lattice constants, as it would correspond to $CoMn_2O_4$ (Figure 1d). H_2 temperature programed reduction (TPR) analysis showed the main Mn_3O_4 reduction peak (380 °C) and an additional peak (480 °C) which can be associated to the reduction of the $CoMn_2O_4$ phase (Figure 1e).[8]

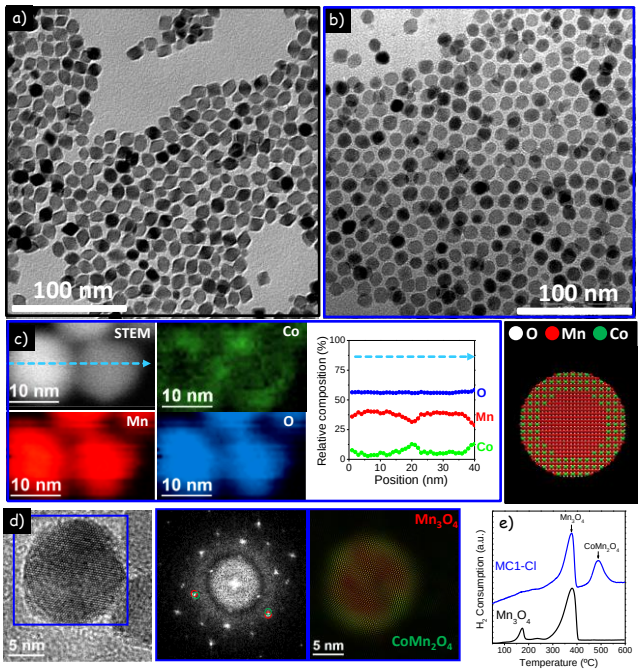

Figure 1. a)-b) TEM micrographs of Mn_3O_4 NPs (a) and MC1-Cl NPs (b). c) HAADF-STEM image and EELS elemental mapping of MC1-Cl NPs and compositional line profile of Mn, Co and O elements recorded along the lines shown in the STEM images. d) HRTEM micrograph of a MC1-Cl NP, details of the red and green squared regions with corresponding power spectra, and colorful structural map showing the distribution of Mn_3O_4 (green) and $CoMn_2O_4$ (red) phases. e) H_2 TPR profile of Mn_3O_4 and MC1-Cl NPs

When cobalt perchlorate ($Co(ClO_4)_2 \cdot 6H_2O$) instead of chloride was used as cobalt precursor, NPs with rougher surfaces were produced (Figure 2a-c). Upon Co perchlorate addition, a clear increase of the NP size was observed, with a final diameter depending on the amount of Co precursor used; from an initial average size of 10.9±0.6 nm, to 15.5±1.3 nm for [Co]/[Mn]=0.5 (MC0.5), ~16.8±1.6 nm for [Co]/[Mn]=1 (MC1) and 17.1±1.9 nm for [Co]/[Mn]=2 (MC2). HRTEM and EELS mapping (figure 2d-e) displayed a clear core-shell type composition distribution with a central core phase and composition consistent with Mn_3O_4. At the NP surface, several crystallite with a CoO phase and an epitaxial relation with the core were evidenced (Figure 2e). H_2 TPR analysis also showed the Mn_3O_4- and the $CoMn_2O_4$-related components and an additional peak at the reduction temperatures of CoO or Co_3O_4 (300 °C, Figure 2f).[9] X-ray photoelectron spectroscopy (XPS) analysis showed Co^{2+} to be the main Co component in all the NPs studied (SI, Figure SI3).

We conclude that with both Co precursors a partial cation exchange between Mn and Co takes place at the outer surfaces of the Mn_3O_4 to form a $CoMn_2O_4$ shell. Besides, the very low coordination ability of perchlorate promoted a high reactivity of the Co ions in solution, which resulted in the nucleation of an additional cobalt oxide phase, identified as CoO, at the NP surface. On the other hand, the lower reactivity of Co^{2+} in the presence of chlorine ions prevented the nucleation of new crystals and constrained the Co incorporation to a partial cation exchange reaction self-limited to a shell thickness of 2-3 nm.

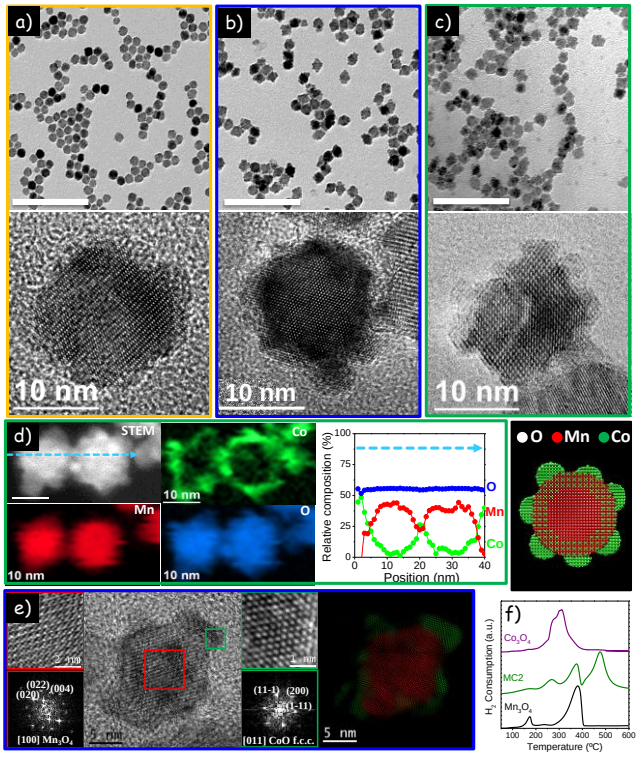

Figure 2. a)-c) TEM (scale bar = 100 nm) and HRTEM micrographs of NPs with compositions: a) MC0.5, b) MC-1, and c) MC2 produced using Co perchlorate. d) HAADF-STEM image and EELS elemental mapping of MC2 NPs and compositional line profile of Mn, Co and O elements recorded along the line shown in the STEM image. d) HRTEM micrographs of a MC1 NP, details of the red and green squared regions with the corresponding power spectra, and colorful structural map showing the distribution of body centered tetragonal Mn_3O_4 (red) and face centered cubic CoO (green) phases. f) H_2 TPR profile of Mn_3O_4, MC02 and Co_3O_4 NPs

To study their electrocatalytic properties toward ORR and OER, NPs were supported on carbon powder (Vulcan XC-72) with a weight ratio of 30% (NP/C) through sonication of NPs and carbon in chloroform and ethanol (1:1). NP/C nanocom-

posites were activated via thermal annealing under air atmosphere at 180 °C for 5 h (SI). BET analysis of NP/C showed around 140 m^2/g and 20 nm of specific surface area and average pore size, respectively (Table S1). No appreciable change was observed from TEM characterization and XRD patterns, indicating insignificant NP structural and size variation (SI).

ORR activity of NP/C was measured in O_2-saturated 0.1 M KOH aqueous solution using a rotating disk electrode (RDE, Figures S8 and S9). Figure 3a shows linear sweep voltammograms (LSV) of the MC/C, reference Mn_3O_4/C and Co_3O_4/C and commercial Pt/C electrocatalysts. The LSVs under N_2-saturated electrolyte did not give any significant current (Figure S9) Figure 3b displays two ORR figures of merit, the current density at half–wave potential and the required potentials to reach -3 mA.cm^{-2}. Yet, an extended electrochemical data is given in Table 1. MC1/C catalyst outperformed the rest, showing highest half-wave and on-set potential, 0.80 and 0.92 V vs. RHE which is higher than MC1-Cl/C and reference samples. Higher CoO concentrations (MC2/C) maintained the maximum current density in the diffusion limited region but resulted in lower current values at the half-wave potential.

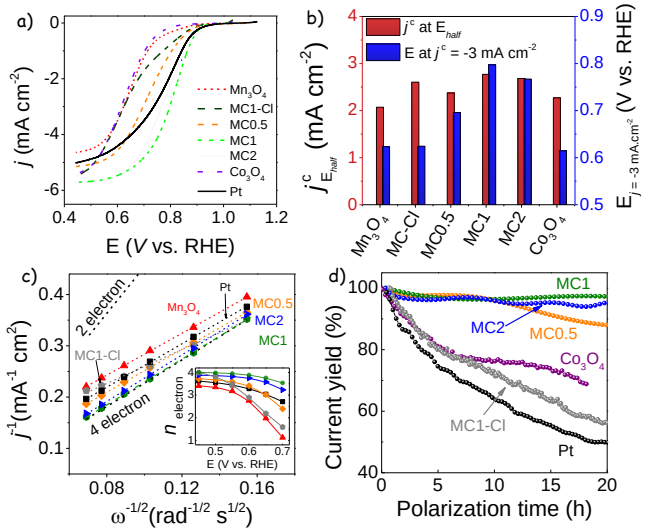

Figure 3. (a) ORR polarization curves of MC/C, Mn_3O_4/C, Co_3O_4/C and Pt/C in O_2-saturated 0.1 M KOH at 1600 rpm using a scan rate of 5 mV/s. (b) Kinetic current densities at half-wave potential and required potentials for j_k= 3 mA cm^{-2}. (c) K-L plots at 0.5V *vs.* RHE. The standard lines for 2 and 4 electron pathways are also plotted as a guideline. Inset shows n_t at different potentials. d) Chronoamperometric responses at 0.8 V in O_2-saturated 0.1 M KOH.

Tafel values obtained from a low ORR current density range, where the limitation by O_2 diffusion in the active layer is negligible, were considered for comparison (Figure 3c). MC1/C exhibited a Tafel value of 52 mV.dec^{-1}, much lower than MC1-Cl/C (95 mV dec^{-1}), Mn_3O_4/C (159 mV.dec^{-1}), Co_3O_4/C (124 mV.dec^{-1}) and benchmark Pt/C (76 mV.dec^{-1}), indicating a higher activity with favorable kinetics. The electron transfer number (n_t) was calculated by Koutecky-Levich (K-L) method from the RDE current-potential curves at various rotation speeds (Figures S8 and S10). Figure 3d shows n_t as a function of electrode potential from the slope of the resulting best-fit line i.e. 0.45-0.7V. These results demonstrate the incorporation of CoO nanocrystallites facilitates rapid electron transfer shifting the ORR mechanism towards the 4-electron pathway, via n_t value from 3.35 for bare Mn_3O_4/C and 3.43 for Mn_3O_4@$CoMn_2O_4$/C, to 3.68, 3.98 and 3.86 at 0.5 V vs. RHE for MC0.5/C, MC1/C and MC2/C, respectively.[10]

In terms of stability, MC/C catalysts showed current retention above 95% (MC1/C) of the initial current after 20 h. This is an outstanding value compared with benchmark Pt/C catalyst under ORR, losing nearly half of its current density within the first 20 hours and 70% after 60 hours test (Figure 4c and Figure S11) which could be a reason of high number of contact sites between Pt NPs and carbon support leading to faster oxidation of carbon materials as shown in a recent work.[11] Besides, as discussed earlier, the 4-electron O_2 reduction into OH^- can compete with the 2-electron pathway yielding HO_2^- species which are detrimental to the ORR performance, generating problems like membrane alteration or electrode materials corrosion.[14] As shown in Figure 3d, MC1-Cl exhibited a lower electron transference value which is an evidence of peroxide formation. In contrast, for MC1 and MC2, n_t values close to 4 revealed a direct O_2 reduction path, plus an advanced decomposition activity against deteriorating peroxide species, which is beneficial for holding a stable catalytic activity.

Catalytic activities for OER are shown in Figure 4a, which exhibit their linear sweeps driven to higher values than water oxidation standard potential, 1.23 V vs. RHE along with the corresponding Tafel plots displayed inFigure 4b. MC/C and particularly MC1/C, also outperformed reference electrocatalysts in the OER. For MC1/C, oxidative current started at 1.54 V vs. RHE, reaching up to a current density of 15 mA·cm^{-2} at 1.76 V, with a sharp increase. Co_3O_4/C is in state-of-art giving an excellent catalytic activity, clearly outperforming that of Pt/C and Mn_3O_4/C. At higher current densities, Pt/C exhibited a break in the slope implying a change in the structure owing to oxidation of Pt and carbon support following degradation and dissolution.[12] Therefore, an IrO_2-based comercially available anode (EC Electrochemical Cell, Ti/IrO_2:Ta_2O_5 DSA) was also tested here as OER benchmark catalyst. The linear polynomial regression of the data obtained from LSVs showed the MC1/C to exhibit the faster reaction kinetics, with a Tafel value of 95.2 mV per decade comparable to benchmark DSA electrode.

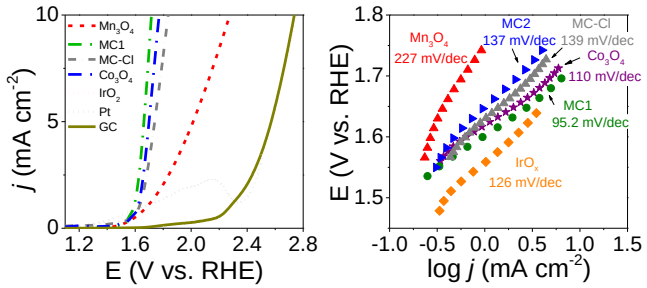

Figure 4. (a) OER polarization curves of MC/C, Pt/C and DSA in O_2-saturated 0.1 M KOH at a scan rate of 5 mV/s. (b) Tafel plots derived from OER polarization curves.

A main figure of merit for practical electrochemical and photoelectrochemical applications is the difference between the potential at ORR current density of -3 mA·cm^{-2} and that at OER current density of 10 mA·cm^{-2} ($\Delta E_{ORR-OER}$, Table 1).[2d] The smaller this difference, the closer a material is to being

an ideal reversible catalyst. This value was 2.17 for Mn_3O_4/C and 2.01 for Pt/C, mainly due to low OER performances. Much lower $\Delta E_{ORR-OER}$ values were obtained for Co_3O_4, 1.15 V, and especially for MC1/C, 0.92 V, which is among the best values reported (SI, Table 2). As a reference, taking the values of Pt as standard ORR catalysts and DSA for OER, a $\Delta E_{ORR-OER}$=1.01 V would be obtained.

Besides, MC/C electrocatalysts also showed excellent stability, a critical requirement for practical application. LSV before and after a 20 hours test, showed no significant change either in the on-set voltage or in current density of both ORR and OER for MC0.5/C, MC1/C and MC2/C electrocatalyts. Even a slight improvement was observed in the OER catalysis current density probably due to the increased wetting by penetration of the electrolyte into the nanopores/voids of the thin-film (Figure 4d).

Table 1. Summary of the ORR/OER Catalytic Performance Revealed from Tafel Plots and Koutechky-Levich plots

	ORR				OER		ORR-OER
	η	$j_{l,c}$	n_t		η	E	ΔE**
	E – Eeq V	mA.cm^{-2}			E – Eeq V	j=10mAcm^{-2} V	V
Mn_3O_4/C	0.35	-4.64	3.2		0.43	2.8	2.17
MC-Cl/C	0.34	-5.20	3.5		0.43	1.84	1.21
MC0.5/C	0.38	-5.14	3.6		0.38	*1.95	1.25
MC1/C	0.31	-5.71	3.9		0.31	1.72	0.92
MC2/C	0.34	-5.73	3.8		0.35	*1.90	1.33
Co_3O_4/C	0.41	-5.40	3.4		0.39	1.77	1.16
Pt/C	0.33	-5.25	3.4	**DSA**	0.25	1.75	$^{\Delta}$ 1.01

* Due to the interaction of carbon near 2V; this value was obtained by linear regression of Tafel & LSV plot. ** Difference between the potential at ORR current density of -3 mA·cm^{-2} and that at OER current density of 10 mA cm^{-2}. $^{\Delta}$ Value taken from Pt ORR and DSA OER.

In summary, Mn_3O_4@$CoMn_2O_4$-CoO NPs with controlled composition were synthesized at low temperature and air atmosphere involving the cation exchange of Mn by Co in preformed Mn_3O_4 NPs and the simultaneous nucleation of CoO nanocrystallites on the NP surface. When employed as electrocatalysts for the ORR and OER in alkaline media, such hetereostructured NPs showed activities outperforming Mn_3O_4, Co_3O_4, and benchmark electrocatalysts. In particular, the optimized MC1 composition showed exceptional properties as bifunctional ORR/OER electrocatalyst including high current densities with excellent overall oxygen electrode activity and an improved durability.

ASSOCIATED CONTENT

Supporting Information

Additional experimental, characterization details, additional compositional maps and HRTEM and TEM images, TGA analysis and BET measurement. This material is available free of charge via the Internet at http://pubs.acs.org.

AUTHOR INFORMATION

Corresponding Author

* acabot@irec.cat

Author Contributions

‡These authors contributed equally.

Notes

The authors declare no competing financial interests.

ACKNOWLEDGMENT

This work was supported by the European Regional Development Funds, the Framework 7 program under project UNION (FP7-NMP-2012-310250) and the Spanish MINECO Project BOOSTER (ENE2013-46624-C4-3-R). ZL thanks the China Scholarship Council for scholarship support. EI and MI thank AGAUR for their Beatriu de Pinós postdoctoral grant (2013 BP-A00344) and PhD grant, respectively. Authors also acknowledge the funding from Generalitat de Catalunya 2014 SGR 1638.

REFERENCES

(1) (a) Flox, C.; Rubio-Garcia, J.; Nafria, R.; Zamani, R.; Skoumal, M.; Andreu, T.; Arbiol, J.; Cabot, A.; Morante, J. R., *Carbon* 2012, 50, 2372-2374. (b) Herranz, T.; Ibáñez, M.; Gomez de la Fuente, J. L.; Perez-Alonso, F. J.; Pena, M. A.; Cabot, A.; Rojas, S. *ChemElectroChem* 2014, 1, 885-895. (c) Porter, N. S.; Wu, H.; Quan, Z.; Fang, J. *Acc. Chem. Res.* 2013, *46*, 1867-1877.

(2) (a) Chen, D.; Chen, C.; Baiyee, Z. M.; Shao, Z.; Ciucci F. *Chem. Rev.* 2015, 115, 9869-9921. (b) Liang, Y. Y.; Li, Y. G.; Wang, H. L.; Dai, H. *J. Am. Chem. Soc.* 2013, 135, 2013-2036. (c) Li, C.; Han, X.; Cheng, F.; Hu, Y.; Chen, C.; Chen, J. *Nat. Commun.* 2015, 6, 7345, DOI.10.1038/ncomms8345 (d) Gorlin, Y.; Jaramillo, T. F. *J. Am. Chem. Soc.* 2010, 132, 13612-13614.

(3) (a) Zhu, H.; Zhang, S.; Huang, Y.; Wu, L.; Sun, S. *Nano Lett.* 2013, 13, 2947-2951. (b) Cheng, F.; Shen, J.; Peng, B.; Pan, Y.; Tao, Z.; Chen, J. *Nat. Chem.* 2011, 3, 79-84.

(4) (a) Wang, D.; Chen, X.; Evans, D. G.; Yang, W. *Nanoscale* 2013 , 5 , 5312-5315. (b) Rahman, M. M.; Khan, S. B.; Gruner, G.; Al-Ghamdi, M. S.; Daous, M. A.; Asiri, A. M. *Electrochim. Acta* 2013, 103, 143-150. (c) Pang, H.; Deng, J. W.; Du, J. M.; Li, S. J.; Li, J.; Ma, Y. H.; Zhang, J. S.; Chen, J. *Dalton Trans.* 2012, 41, 10175-10181.

(5) (a) Bidault, F.; Brett, D. J. L.; Middleton, P. H.; Brandon, N. P. *J. Power Sources* 2009, 187, 39-48. (b) Du, J.; Pan, Y.; Zhang, T.; Han, X.; Cheng, F.; Chen, J. *J. Mater. Chem.* 2012, 22, 15812-15818.

(6) (a) Liang, Y.; Li, Y.; Wang, H.; Zhou, J.; Wang, J.; Regier, T.; Dai, H. *Nat. Mater.* 2011, 10, 780-786. (b) Liang, Y.; Wang, H.; Zhou, J.; Li, Y.; Wang, J.; Regier, T.; Dai, H. *J. Am. Chem. Soc.* 2012, 134, 3517-3523. (c) Zhao, A. Q.; Masa, J.; Xia, W.; Maljusch, A.; Willinger, M. G.; Clavel, G.; Xie, K. P.; Schlogl, R.; Schuhmann, W.; Muhlert, M. *J. Am. Chem. Soc.* 2014 , 136, 7551-7554. (d) Tompsett, D. A.; Parker, S. C.; Islam, M. S. *J. Am. Chem. Soc.* 2014, 136, 1418-1426.

(7) (a)Yu, T.; Moon, J.; Park, J.; Park, Y. I.; Na, H. B.; Kim, B. H.; Song, I. C.; Moon, W. K.; Hyeon, T. *Chem. Mater.* 2009, 21, 2272-2279. (b) Oh, M. H.; Yu, T.; Yu, S.-H.; Lim, B.; Ko, K.-T.; Willinger, M.-G.; Seo, D.-H.; Kim, B. H.; Cho, M. G.; Park, J.-H.; Kang, K.; Sung, Y.-E.; Pinna, N.; Hyeon, T. *Science* 2013, 340, 964–968.

(8) (a) Hosseini, S.A.; Niaei, A.; Salari, D.; Nabavi, S.R. *Ceram. Int.* 2012, 38, 1655-1661. (b) Hosseini, S.A.; Salari, D.; Niaei, A.; Deganello, F.; Pantaleo, G.; Hojati, P. *J. Environ. Sci. Health., Part A* 2011, 46, 291-297.

(9) (a) van Steen, E.; Sewell, G. S.; Makhothe, R. A.; Micklethwaite, C.; Manstein, H.; de Lange, M.; O'Connor, C. T. *J. Catal.* 1996, 162, 220-229. (b) Lin, H. Y.; Chen, Y. W. *Mater. Chem. Phys.* 2004, 85, 171–175. (c) *Sexton, B.; Hughes, A.; Turney, T. J. Catal. 1986, 97, 390-406*. (d) Brown, R.; Cooper, M.; Whan, D. *Appl. Catal.* 1982, 3, 177-186.

(10) Bard. A. J.; Faulkner, L. R. Electrochemical Methods: Fundamentals and Applications, 2nd ed.; Wiley New York, 2001.

(11) Kou, Z.; Cheng, K.; Wu, H.; Sun, R.; Guo, B.; Mu, S. *ACS Appl. Mater. Interfaces* DOI: 10.1021/acsami.5b11086.

(12) Gherevko, S.; Zeradjanin, A. R.; Keeley, G. P.; Mayrhofer, K. J. J. *Electrochem. Soc.* 2014, 161, H822-H830.